CrossMark

ORIGINAL RESEARCH

Impaired topological architecture of brain structural networks in idiopathic Parkinson's disease: a DTI study

Changhong Li[1] · Biao Huang[2] · Ruibin Zhang[1] · Qing Ma[1] · Wanqun Yang[2] ·
Lijuan Wang[3] · Limin Wang[3] · Qin Xu[1] · Jieying Feng[2] · Liqing Liu[1] ·
Yuhu Zhang[3] · Ruiwang Huang[1]

Abstract Parkinson's disease (PD) is considered as a neuro-degenerative disorder of the brain central nervous system. But, to date, few studies adopted the network model to reveal topological changes in brain structural networks in PD patients. Additionally, although the concept of rich club organization has been widely used to study brain networks in various brain disorders, there is no study to report the changed rich club organization of brain networks in PD patients. Thus, we collected diffusion tensor imaging (DTI) data from 35 PD patients and 26 healthy controls and adopted deterministic tractography to construct brain structural networks. During the network analysis, we calculated their topological properties, and built the rich club organization of brain structural networks for both subject groups. By comparing the between-group differences in topological properties and rich club organizations, we found that the connectivity strength of the feeder and local connections are lower in PD patients compared to those of the healthy controls. Furthermore, using a network-based statistic (NBS) approach, we identified uniformly significantly decreased connections in two modules, the limbic/paralimbic/subcortical module and the cognitive control/attention module, in patients compared to controls. In addition, for the topological properties of brain network topology in the PD patients, we found statistically increased shortest path length and decreased global efficiency. Statistical comparisons of nodal properties were also widespread in the frontal and parietal regions for the PD patients. These findings may provide useful information to better understand the abnormalities of brain structural networks in PD patients.

Keywords Rich club organization · Diffusion tensor imaging · Edge architecture · Network-based statistic

✉ Biao Huang
cjr.huangbiao@vip.163.com

✉ Ruiwang Huang
ruiwang.huang@gmail.com

1 Center for the Study of Applied Psychology, Key Laboratory of Mental Health and Cognitive Science of Guangdong Province, School of Psychology, Brain Study Institute, South China Normal University, Guangzhou 510631, People's Republic of China

2 Department of Radiology, Guangdong Academy of Medical Sciences, Guangdong General Hospital, Guangzhou, People's Republic of China

3 Department of Neurology, Guangdong Academy of Medical Sciences, Guangdong General Hospital, Guangzhou, People's Republic of China

Introduction

Parkinson's disease (PD), a chronic neurodegenerative disease of the central nervous system, is clinically characterized by resting tremor, muscle rigidity, bradykinesia, and other abnormal postures and pace (Jankovic 2008; Lees et al. 2009). Besides motor deficits, PD patients also usually experience cognitive declines and visual impairments (Chaudhuri et al. 2006; Diederich et al. 2009). According to previous neurobiological studies (Dauer and Przedborski 2003; Drui et

al. 2014), the main pathogenesis of Parkinson's disease begins in the basal ganglia, and then results in widespread brain abnormalities in PD patients. However, no study has reported abnormal topological properties of brain structural networks in PD patients.

Diffusion tensor imaging (DTI) is an available non-invasive technique to detect white matter (WM) microstructures of the human brain and to estimate connectivity strength between distinct regions in vivo (Le Bihan and Johansen-Berg 2012). Most previous PD-related DTI studies (see the summary in Table 5) focused on detecting alterations in some specified regions or WM tracts indicated by fractional anisotropy (FA) and mean diffusivity (MD). For instance, Karagulle et al. (2008) found lower FA values in the bilateral frontal cortices, supplementary motor area, and anterior cingulum in PD patients. Agosta et al. (2014) found widely decreased FA values in the bilateral superior longitudinal fasciculus, corona radiata, corpus callosum, and uncinate fasciculus of PD patients with cognitive deficits, compared to PD patients without remarkable cognitive deficits. Although these studies provide us a better understanding of the white matter structural alteration in PD, most of them were limited to only detecting the alterations in some specified regions or WM tracts by mapping the alteration of FA and MD, or focused on some specified white matter structural connectivity.

The human brain can be modeled as a network and its topological properties, such as the small-worldness, hub regions, and modules, can be estimated with graph theory (Rubinov and Sporns 2010). Graph theory has been adopted in previous studies (Zalesky et al. 2011; Wang et al. 2013; Tewarie et al. 2014) exploring the abnormal network properties in various brain diseases, including Alzheimer's disease, multiple sclerosis, and schizophrenia. For PD patients, the descriptions of brain structural network can offer us the possibilities of more systematical analysis of specific brain circuits. Noticeably, recent studies (van den Heuvel and Sporns 2011; Kocher et al. 2015) also proposed that brain networks contain a rich club organization, comprised of highly interconnected regions (namely "hubs") and can be used to represent a core neuropathology characteristic of neuropsychiatry (Crossley et al. 2014). The rich club connections that constituted among central hub regions form a backbone of global communication. Several multimodal studies (van den Heuvel et al. 2013; Ball et al. 2014; Daianu et al. 2015; Harrington et al. 2015) using the concept of rich club organization have estimated their changes in brain networks across various populations. For instance, Ball et al. (2014) revealed significant disruptions in short-distance cortico-coritical connections (more specified to the connections among non-hub regions) in a premature cohort. Daianu et al. (2015) suggested those connections among hub regions were relatively preserved, while connections among low-degree regions were significantly disrupted in the Alzheimer's disease patients.

However, few studies explored the changes of brain structural networks in PD patients, especially the rich club organizations in PD patients.

With the aim of uncovering abnormal topology of brain networks in PD patients, we constructed brain structural networks for both the patients and controls, and then compared their differences in both topological properties and rich club organizations. Using a network-based statistic (NBS) approach, we identified the disrupted structural connections in PD patients. Moreover, we assessed the robustness of our findings by using different definitions of edge weights, thresholds of streamline counts, and brain parcellation schemes.

Materials and methods

Subjects

Thirty-five idiopathic PD patients (18 F / 17 M, age = 61.26 ± 11.02 years) were recruited between August 2011 and April 2013 from the Guangdong General Hospital in Guangzhou. All patients underwent a standardized clinical examination by two neurologists (LW and YZ) who have specialized in diagnosing movement disorders for more than 10 years. In this study, the PD patients fulfilled the clinical diagnostic criteria of the UK Parkinson's Disease Society Brain Bank (Daniel and Lees 1993). All patients had an obvious delay in movement initiation, and their clinical behavior performances were recorded in detail (Table S1 in supplementary materials). The severity of disease for each patient was evaluated by using the third part of Unified Parkinson's Disease Rating Scale (UPDRS-III) and the Hoehn and Yahr scale (H-Y stages, Table S2). The general cognitive abilities for all patients were assessed by using the Chinese Version of the Mini-Mental State Examination (MMSE). The exclusion criteria for the PD patients were as follows: (i) PD caused by other psychiatric and neurological disorders, such as brain stroke, traumatic brain injury, and brain tumor; (ii) taking any antipsychotics; (iii) patients with a progressive supranuclear palsy or multiple system atrophy; and (iv) patients with a MMSE score < 25 because subjects with such low scores were considered to have the cognitive impairments. Additionally, we enrolled 26 healthy subjects as the controls (16 F / 10 M, age = 62.81 ± 10.80 years). The inclusions for the controls were: (i) no history of neurological or psychiatric disorders or brain injuries, and (ii) MMSE score ≥ 25. Table 1 lists the demographic information for all the PD patients and the controls. All subjects were right-handed according to their self-report. The protocol was approved by the Medical Research Ethical Committee of the Guangdong General Hospital. Written informed consent was obtained from each subject prior to the study. Under the care of clinical neurologists, the PD patients

Table 1 Basic demographics and clinical characteristics of the patients with Parkinson's disease (PD) and the healthy controls (HC) in this study

Characteristics	PD ($n = 35$)	HC ($n = 26$)	p-value
Gender (Male/Female)	18 / 17	16 / 10	0.43
Age (years)	61.26 ± 11.02	62.81 ± 10.08	0.31
MMSE	27.03 ± 2.28	28.46 ± 1.82	0.02[*]
UPDRS-III	30.04 ± 9.73	NA	NA
H-Y stages, no. (mean ± SD)			
Range: 1–2	7 (1.14 ± 0.24)	NA	NA
Range: 2–3	22 (2.18 ± 0.25)	NA	NA
Range: 3	6 (3 ± 0.00)	NA	NA
Damaged body part, No. (%)			
LB	4 (11 %)	NA	NA
RB	14 (40 %)	NA	NA
LB & RB	17 (49 %)	NA	NA
Disease duration, No. (mean ± SD)			
0–5 years	25 (1.82 ± 1.15)	NA	NA
5–10 years	10 (7.70 ± 2.16)	NA	NA

Abbreviations MMSE Mini-Mental State Examination, *UPSRS-III* Unified Parkinson Disease Rating Scale-III, *H-Y* Hoehn and Yahr scale, *LB (RB)* left (right) body part, *NA* not applicable, *%* percentage relative to whole population of the group

who used medications were requested to stop taking any medications for about 12 h before the MRI scanning.

Data acquisition

All MRI data were acquired on a 3T GE MRI scanner with a standard 8-channel phased-array receiver-only head coil at the Guangdong General Hospital. The DTI data for each subject were acquired using a spin-echo diffusion-weighted EPI sequence with the following parameters: repetition time (TR) = 15,275 ms, echo time (TE) = 75 ms, flip angle (FA) = 90°, field of view (FOV) = 320×320 mm^2, data matrix = 128×128, 25 diffusion-sensitive directions with b value = 1000 s/mm^2 and a volume of non-diffusion weighting (b_0) images, slice thickness = 2.5 mm, and 60 axial slices without gap covering the whole-brain. We also acquired high-resolution T1-weighted 3D using rapid interference phase gradient echo flip recovery pulse sequence (FSPGRUSR). The imaging parameters were: TR/TE = 8.4/3.3 ms, FA = 13°, FOV = 240×240 mm^2, matrix size = 256×256, slice thickness = 1 mm, voxel size = $0.94 \times 0.94 \times 1$ mm^3, and 146 sagittal slices covering the whole-brain.

Data preprocessing

By using the FSL/FDT Toolbox (Version 5.0; www.fmrib.ox. ac.uk/fsl), we first corrected the eddy current by realigning all the diffusion-weighted images to the b_0 images, and then

stripped non-brain tissue from the whole head to reduce the intensity inhomogeneity for each individual DTI data. Then, we processed the corrected DTI data with DTIStudio (Version 3.0.2; https://www.mristudio.org). The WM streamlines for the whole-brain were built based on the Fiber Assignment by Continuous Tracking (FACT) algorithm (Mori and van Zijl 2002), a deterministic tractography approach implemented in DTIStudio. Fiber tracking was terminated at voxels where $FA < 0.2$ or where the angle between two eigenvectors to be connected by the tracking was greater than 45°.

Network construction

Brain structural network was constructed for each subject according to the Automatic Anatomical Label (AAL) atlas (Tzourio-Mazoyer et al. 2002), which parcellates the whole-brain into 90 regions and is referred to as AAL-90 (Table S2 in supplementary materials). Following previous studies (Gong et al. 2009; Zhang et al. 2015), we took each brain region as a node and the inter-regional WM streamline as the edge to construct a 90-by-90 matrix. To reduce the potential effect of noise or other factors during diffusion tractography caused by data acquirement, preprocessing or processes, we followed previous studies (Lo et al. 2010; Shu et al. 2011) to set a threshold of streamline counts to ensure the major connections among cortical regions. That is, we assumed that any pair of regions i and j were connected if the number of streamlines (NOS) was at least three, or $NOS \geq 3$, between these two regions, and took the mean FA value along the inter-regional streamlines as the edge weights. In this way, we constructed a FA-weighted brain structural network for each subject (the details described in the supplementary materials).

Network analysis

Edge architecture

The edge architecture of brain networks can be characterized by using a rich club organization, which is defined as those connections among hub regions ("rich club"). The "rich club" refers to nodes with higher degrees within brain networks and a higher connectivity strength of inter-nodal connections compared to those composed by randomly selected brain regions (van den Heuvel et al. 2012). We constructed the group-averaged FA-weighted structural connectivity network for each group. In brief, for a given subject group, we first retained the inter-nodal connections of each of these connections was presented in at least 50 % of all the subjects, and then averaged all values for each connection to generate the group-averaged FA-weighted network for this group. In this study, we used the equation that appeared in Tian et al. (2011) to calculate the integrated rich club, feeder and local connections, respectively.

The rich club nodes and the rich club organization were determined according to the following four steps. Step-1, we determined the value of degree k for a node i, counting the number of connections that the node i shared with other nodes in the group-averaged network. For the degree value k, we removed the nodes whose degree $\leq k$ from the group-averaged network and selected the remaining nodes as the prominent nodes. Step-2, we calculated the number of connections $E > k$ for those among the selected prominent nodes that were connected with each other, and obtained the sum of the edge weights (i.e., sum of FA values), W, of these inter-nodal connections. Step-3, we ranked all of the edge weights (or elements of the group-averaged FA-weighted matrix) in descending order of their values to generate a vector W^{ranked}. We also estimated the sum of the edge weights (or sum of FA values) for those strongest connections in the W^{ranked}, which has the same number as the connections $E > k$ of Step-2. Step-4, we calculated the rich club coefficient $\phi^w(k)$ for the group-averaged FA-weighted network, which is given by the ratio of the results from Step-2 and Step-3 by the following equation:

$$\phi^w(k) = \frac{W_{>k}}{\sum_{l=1}^{E_{>k}} W_l^{ranked}}, \tag{1}$$

where the superscript 'w' indicates the FA-weighted network. We also calculated the normalized rich club coefficient $\phi_{norm}^w(k)$ by:

$$\phi_{norm}^w(k) = \frac{\phi^w(k)}{\phi_{rand}(k)} \tag{2}$$

where $\phi_{rand}(k)$ is the averaged rich club coefficient over 5,000 random networks, each preserving the same numbers of nodes, strength, and degree distribution as the real brain network (Rubinov and Sporns 2010). Finally, we computed $\phi_{norm}^w(k)$ at each level of degree k. Using a nonparametric permutation t-test, we determined the statistical significances of these normalized rich club coefficients between the PD patients and the controls by following a previous study (van den Heuvel and Sporns 2011).

For a specified value of degree k, a network is considered to have a rich club organization if $\phi_{norm}^w(k) > 1$. Following previous studies (Collin et al. 2014a, b), we referred those brain regions whose degrees greater compared to a specified value k as "rich club" nodes, while the remaining brain regions as the non-rich club nodes. Based on these categorizations, the edges of the whole-brain network was classified into three types of connections (Collin et al. 2014a): (i) "rich club" connections, connecting rich club nodes to each other, (ii) "feeder" connections, connecting rich club nodes to non-rich club nodes, and (iii) "local" connections, connecting non-rich club nodes to

each other. For a specified degree k, we calculated the connectivity strength for each type of connections in the brain structural networks. That is, all of the FA values belonging to rich club connections (RC), feeder connections ($Feeder$), and local connections ($Local$) were separately collected. Using the permutation t-test, we compared the between-group difference in the connectivity strength for each type of the rich club, feeder, and local connections. In order to detect the between-group differences in the length of streamlines (unit: mm) between the PD patients and the controls, we also generated the length of streamlines and compared them (see supplementary materials for details).

Although the statistical test can be used to test the existence of rich club organization in human brain networks, variances in the selected k value might affect the choices of rich club and non-rich club nodes of brain networks. This may result in variances of the between-group comparisons in any of the three types of connections. To avoid the effects of different selected degree k on network analyses, we used the integrated rich club connections (RC^{int}), integrated feeder connections ($Feeder^{\mathrm{int}}$), and integrated local connections ($Local^{\mathrm{int}}$) across the range of degrees from 16 to 21 rather than the connectivity strength of RC, $Feeder$, and $Local$ at a specified degree k to compare the between-group differences. According to a previous study (Tian et al. 2011), the integrated rich club, feeder and local connections were defined as summations:

$$X^{\mathrm{int}} = \sum_{k=16}^{25} X(k\Delta s)\Delta s, \tag{3}$$

where X can be represented any of the rich club connection (RC), feeder connection ($Feeder$), or local connection ($Local$) at as specified degree k whose $\phi_{norm}^w(k) > 1$ ($16 \leq k \leq 21$ in our study, please see Fig. 1a). The degree interval was $\Delta s = 1$. For each group, the FA values or length of streamlines corresponding to RC^{int}, $Feeder^{\mathrm{int}}$, and $Local^{\mathrm{int}}$ were calculated according to Eq. (3).

Network parameters

Global properties of brain networks can be characterized by the following seven parameters: clustering coefficient (C_p), shortest path length (L_p), global efficiency (E_{glob}), local efficiency (E_{loc}), normalized clustering coefficient (γ), normalized shortest path length (λ), and small-worldness (σ). We utilized three parameters γ, λ, and σ, to measure the small-world property. For a given network, if $\gamma > 1$ and $\lambda \approx 1$, or $\sigma > 1$, we regarded this network as a small world network (Watts and Strogatz 1998). The definitions and interpretations for all of these global parameters are given in Table 2.
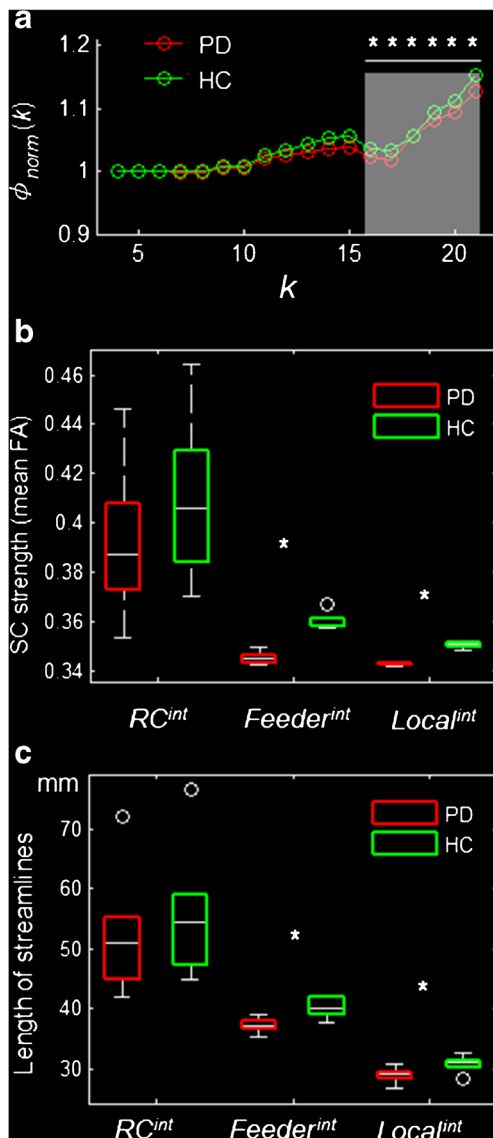
Fig. 1 Comparison of rich club organization between the PD patients and the healthy control (HC). **a** Normalized rich club coefficient, $\phi_{norm}^{w}(k)$. Each symbol "○" in red (blue) indicates the normalized rich club coefficient for the patients (controls) at a specific degree k. The light white area indicates $\phi_{norm}^{w}(k) > 1$ from degrees $k = 16$ to 21 for both the PD patients and the controls. **b** Integrated local connections, $Local^{int}$, integrated feeder connections, $Feeder^{int}$, and integrated rich club connections, RC^{int}. We found significant between-group differences in both $Local^{int}$ and $Feeder^{int}$, but not in RC^{int}. **c** Box plot of streamline lengths for three types of integrated connections. The PD patients had significantly deceased length of streamlines in the $Feeder^{int}$ and $Local^{int}$, but not in the RC^{int}, compared to the controls. The *asterisk* (*) indicates a significant between-group difference at $p < 0.05$. The *top and bottom of a box plot* indicate 25 and 75 % percentiles across all values of each group, the middle line of a box plot represents 50 % percentile. The *top and bottom of white line outside a box plot* indicate 10 and 90 % percentiles across all values of each group, and outlier is represented by "○"

We also assessed nodal properties of brain structural networks by using the following three parameters: nodal strength (K_i), nodal efficiency (E_i), and nodal betweenness (B_i). Their definitions and interpretations are also listed in Table 2. In this study, both the global and nodal parameters were computed using software packages of BCT (Rubinov and Sporns 2010) and GRETNA (Wang et al. 2015).

Statistical analysis

Comparison of network parameters

First, we conducted a multiple linear regression for each group to regress out the three covariates, the gender, age, and gender-age interaction. Second, we determined significant between-group differences for each of the global and nodal parameters by using a nonparametric permutation t-test (Nichols and Holmes 2002). For a given parameter, we randomly reassigned each subject into any group of the patients or controls letting the two new randomly generated groups generated the same numbers of subjects as the two original groups, and calculated the p-value (two sample two-tailed t-test). This procedure was repeated 5,000 times and resulted in a null distribution of p-values for the given parameter. Thus, the significant two-sided p-value of between-group difference was calculated by its percentile position, that is, the proportion of those p-values that were larger than the real p-value in the 5, 000 repetitions. We set $p < 0.05$ as the level of significant between-group difference for each parameter. In this study, we also respectively examined the statistical significance in RC^{int}, $Feeder^{int}$, and $Local^{int}$ between the PD patients and the controls using the permutation t-test (5,000 repetitions, $p < 0.05$). Similarly, we conducted the same statistical comparisons for length of streamlines between the two groups. In this study, we used the FWE-correction ($p = 0.05$) to correct the false positive results caused by multiple comparisons. Unfortunately, we found non-significant between-group differences in each of these topological parameters when adopting the FEW correction.

Network-based statistic analysis

Network-based statistic (NBS) approach (Zalesky et al. 2010a) was applied to probe those significant different connections between the PD patients and the controls. In short, we first reconfigured brain networks using $p < 0.01$ as the significance level to discover those supra-threshold connections for each connection. Then we determined any connected components and their corresponding size (number of connections). By means of 5,000 randomized repetitions, we obtained the null distribution of the retained maximal size M of the connected components. Following a study of Zalesky et al. (2010b), we assigned the corrected p-value (two-sided) by calculating the proportion of the number of retained maximal size M that exceeded the real M within the null distribution over 5,000 repetitions.

Table 2 Definitions and interpretations of topological parameters for a given network G (N, V)

	Measures	Definitions	Notes
Global parameters	Shortest path length	$L_p(G) = \frac{1}{N(N-1)} \sum_{i=1}^{N} \sum_{j=1, i\neq j}^{N} L_{ij}$	L_{ij} is the shortest path length between node i and node j by using a "harmonic mean" between all pairs of nodes (Watts and Strogatz 1998). $L_p(G)$ can reflect the ability of information transfer in parallel over the whole brain network.
	Global efficiency	$E_{glob}(G) = \frac{1}{N(N-1)} \sum_{i=1}^{N} \sum_{j=1, i\neq j}^{N} \frac{1}{L_{ij}}$	$1/L_{ij}$ represents the reciprocal of the "harmonic mean" of shortest path length. $E_{glob}(G)$ can quantify the global efficiency of the parallel information process.
	Local efficiency	$E_{loc}(G) = \frac{1}{N} \sum_{i=1}^{N} E_{glob}(G_i)$	$E_{glob}(G_i)$ indicates the global efficiency of the subgraph G_i composed of the neighbors of node i. G_i represents a subgraph of G. The local efficiency reflects how much the network is fault tolerant, suggesting how efficient the communication is among the neighbors of node i when it is removed (Latora and Marchiori 2001).
	Clustering coefficient	$C(i) = \frac{2}{k_i(k_i-1)} \sum_{j,k} \left(\overline{w}_{ij}\overline{w}_{jk}\overline{w}_{ki} \right)^{1/3}$	k_i represents the degree of node i. The clustering coefficient C_p of a network is the average of the clustering coefficient over all nodes, which indicates the extent of local interconnectivity or cliquishness in a network (Onnela et al. 2005).
	Small worldness	$\sigma = \frac{\gamma}{\lambda} = \frac{C_p^{real}/C_p^{rand}}{L_p^{real}/L_p^{rand}}$	C_p^{rand} and L_p^{rand} are the averaged values of cluster coefficients and shortest path length of 100 random networks with the same N, V and degree distribution as to the real network. We adopted the Maslovs' wiring algorithm (Rubinov and Sporns 2010).
Nodal parameters	Nodal strength	$K_{nod}(i) = \sum_{j=1, i\neq j}^{N} e_{ij}$	e_{ij} is the edge for the node i with any connected nodes. The strength of a node is the sum of the network strengths across all the nodes over the whole network.
	Nodal efficiency	$E_{nod}(i) = \frac{1}{N-1} \sum_{j=1, i\neq j}^{N} \frac{1}{L_{ij}}$	$E_{nod}(i)$ measures the average shortest path length between a given node i and all of the other nodes in the network. It quantifies the ability of node i in communication transfer within a network.
	Betweenness centrality	$B_{nod}(i) = \frac{1}{(N-1)(N-2)} \sum_{h=1}^{N} \sum_{j=1, h\neq j\neq i}^{N} \frac{\rho_{hj(i)}}{\rho_{hj}}$	$\rho_{hj(i)}$ is the total numbers of shortest path lengths between node h and j which passes through h for a specific node i.

Relationship between network parameters and clinical variables

We examined the relationship between the connectivity of the NBS-derived subnetwork and each of the clinical variables (MMSE score, H-Y scale, duration of diseases, and UPDRS-III score) for the PD patients. More detailed, we calculated the connectivity of NBS-derived subnetwork by averaging FA values of all structural connections derived from NBS approach for each subject. By taking each of the clinical variables (MMSE score, H-Y scale, duration of diseases, and UPDRS-III score) as the independent variable and the connectivity of NBS-derived subnetwork as the dependent variable, we utilized a Spearman's rank order approach to estimate their correlation. The significant level was set at $p < 0.05$. Similarly, we also assessed the relationship between each of the significant changed global or nodal parameters and each of the clinical variables (MMSE score, H-Y scale, duration of diseases, and UPDRS-III score) in the patients. In the calculations, we regressed out three covariates, the gender, age, and gender-age interaction.

Validation: robustness of our main results

The topological properties of brain structural networks may be affected by several factors, mainly included selected definitions of edge weights (Zhong et al. 2015), threshold of NOS in retaining valid network connections (Cheng et al. 2012), and brain parcellation schemes (Wang et al. 2009). In this context, we conducted following strategies to validate the robustness of our main findings.

Definitions of the edge weights For the given two brain regions, if NOS-3, we retained these values as the edge weights; Otherwise we assumed no connections existed between these two regions. Then, we adopted another two definitions of the edge weights to construct the brain networks, and repeated the network analysis. These two definitions were as follows. i) We took the number of streamlines (NOS) as the edge weights. ii) We used the definition of edge weights adopted in Hagmann et al. (2007),

$$w(e) = \frac{2}{s_i + s} \sum_{f \in F_e} \frac{1}{l(f)}, \tag{4}$$

where s_i and s_j represent any two brain regions i and j, F_e represent all streamlines existing these two regions, and $l(f)$ represent the length of streamlines f along its trajectory.

Thresholds of streamline counts To examine the effects of network sparsity on our findings, we took two different values of *NOS* to define the threshold of inter-regional connection, $NOS > 0$ and $NOS \geqq 5$. After re-constructing the whole-brain networks for all subjects, we then repeated the network analysis using same procedures as described in the subsections of "Network construction" and "Network analysis".

Nodes based on different brain parcellation schemes We repeated network analysis by defining the nodes according to two parcellation schemes, the Harvard-Oxford Structural Atlas (HOA-110) (http://fsl.fmrib.ox.ac.uk/fsl/fslwiki/Atlases) and a high-resolution AAL-1,024 atlas. After we obtained a 110-by-110 matrix and a 1,024-by-1,024 matrix, we repeated same procedures as described above. Results were used to test the effect of brain parcellation schemes on network analysis.

Results

Demographic and clinical variables

Table 1 lists the age, gender, MMSE score, and other demographics for both the PD patients and the controls. The PD patients had significantly decreased MMSE score compared to the controls (two-tailed *t*-test, $p = 0.02$). No significant between-group difference was found either in age ($p = 0.31$, two-sided *t*-test) or in gender ($p = 0.43$, χ^2 −test).

Disrupted the edge architecture of PD patients

We found, for both the PD patients and the controls, the normalized rich club coefficients $\phi_{norm}^w(k)$ over the range of degrees k from 16 to 21 (Fig. 1a) were larger than 1 and significant between the two groups. Across a series of degrees k, both the integrated feeder connections ($Feeder^{int}$, $p = 1.29e$-07) and integrated local connections ($Local^{int}$, $p = 6.17e$-06) were significantly decreased in the PD patients compared to the controls (Fig. 1c). No significant between-group difference was found in the integrated rich club connections (RC^{int}, $p = 0.179$) (Fig. 1c). According to Eq. (3), we calculated the connectivity strength of RC^{int}, $Feeder^{int}$, and $Local^{int}$ for both the groups. For each k value, the connectivity strength of RC^{int}, $Feeder^{int}$, and $Local^{int}$ in the PD patients were lower than those of the controls (please see Table 3). In addition, statistical analysis showed that the PD patients had significantly deceased length of streamlines in the $Feeder^{int}$ ($p = 0.0056$) and in the $Local^{int}$ ($p = 0.0258$) but not in the RC^{int} ($p = 0.300$) compared to the controls (Fig. 1d).

Table 3 Selected rich club regions and types of connections (rich club, feeder and local connections) over degrees k from 16 to 21 in both the PD patients and the healthy controls (HC)

Degree k	Rich club regions	Rich club connections			Feeder connections			Local connections		
		PD mean/SD	HC mean/SD	p-value	PD mean/SD	HC mean/SD	p-value	PD mean/SD	HC mean/SD	p-value
16	Bilateral ORBsup, INS, HIP, LING, FFG, PCUN, PUT and ITG; PreCG.R, SFGdor.R, CAL.R, SFGmed.L	0.353/0.074	0.370/0.071	0.090	0.345/0.062	0.358/0.064	0.011	0.342/0.067	0.348/0.070	0.170
17	Bilateral INS, HIP, LING and PCUN; SFGdor.R, ORBsup.L, FFG.L, PUT.R, ITG.L	0.373/0.070	0.384/0.078	0.272	0.345/0.061	0.359/0.061	0.009	0.342/0.067	0.350/0.070	0.069
18	Bilateral SFGdor, LING, and PCUN; SFGdor.R, ORBsup.L, INS.R, PUT.R, ITG.L	0.383/0.070	0.401/0.073	0.199	0.343/0.063	0.358/0.064	0.009	0.343/0.066	0.351/0.069	0.066
19	Bilateral HIP and PCUN; ORBsup.L, LING.R, PUT.R, ITG.L	0.392/0.071	0.412/0.732	0.233	0.343/0.063	0.359/0.064	0.013	0.344/0.066	0.352/0.068	0.047
20	Bilateral HIP and PCUN; LING.R, PUT.R, ITG.L	0.408/0.061	0.430/0.623	0.187	0.346/0.063	0.361/0.065	0.021	0.342/0.066	0.351/0.068	0.037
21	Bilateral HIP and PCUN	0.446/0.030	0.464/0.059	0.263	0.349/0.062	0.367/0.062	0.029	0.343/0.066	0.351/0.068	0.017
p-value	–	–		0.1798	–		1.29e-07	–		6.17e-06

The asterisk (*) indicates significant between-group difference at $p < 0.05$

Abbreviations SFGdor superior frontal gyrus, dorsolateral, *ORBsup* superior frontal gyrus, orbital part, *INS* insula, *HIP* hippocampus, *LING* lingual gyrus, *FFG* fusiform gyrus, *PCUN* precuneus, *PUT* putamen, *ITG* inferior temporal gyrus, *CAL* calcarine fissure and surrounding cortex, *SFGmed* superior frontal gyrus, medial, *PreCG* precental gyrus

Figure 2b shows a significantly decreased structural subnetwork ($p = 0.001$, corrected) that derived from NBS approach in the PD patients compared to the controls. This subnetwork contains 62 nodes (including 20 hub regions when $k > 16$) and 76 inter-nodal connections, which are presented in Fig. 2a and listed in Table S3 (in the supplementary materials). Further correlation analysis indicated that the connectivity strength of the NBS-derived subnetwork in the PD patients was significantly negatively correlated with the duration of disease ($r = -0.434$, $p = 0.013$), as shown in Fig. 2c.

Altered network parameters in PD patients

Figure 3a plots the changed global parameters for both the PD patients and the controls. We obtained $\gamma > 1$ and $\lambda \approx 1$, or $\sigma > 1$, which suggested that both the PD patients and the controls exhibited the small-world attributes. We found significantly decreased E_{glob} ($p = 0.038$) but increased L_p ($p = 0.036$) in the PD patients compared to the controls (Fig. 3a).

We also analyzed the correlations between the global parameters and clinical variables in the PD patients. Figure 3b shows that L_p was significantly positively correlated ($r = 0.55$, $p = 0.001$) but E_{glob} was significantly negatively correlated ($r = -0.55$, $p = 0.001$) with the duration of disease.

We compared between-group differences in nodal parameters. Table 4 lists the identified 16 brain regions with uniformly significantly decreased nodal parameters in the PD patients compared to the controls. Among these regions, five brain regions were located in the right frontal cortex, six in the temporal cortex, and the others in the subcortical, occipital, and parietal cortices.

For the brain regions listed in Table 4, we also performed correlation analyses between the normalized nodal parameters and the clinical variables. Only five brain regions (SFGmed.L, CUN.R, FFG.L, ORBsup.L, and SOG.L) showed their nodal parameters were significantly correlated with the clinical variables in the PD patients (Fig. 4). In SFGmed.L, we found UPDRS-III score was significantly positively correlated not only with the nodal strength K_i ($r = 0.53$, $p = 0.002$) but also with the nodal efficiency E_i ($r = 0.48$, $p = 0.005$). In ORBsup.L, the nodal efficiency E_i was significantly positively correlated with MMSE score ($r = 0.37$, $p = 0.037$). However, in SOG.L, the nodal betweenness B_i was significantly negatively correlated with the duration of disease ($r = 0.40$, $p = 0.025$). The nodal efficiency E_i in CUN.R was significantly positively correlated with UPDRS-III ($r = 0.45$, $p = 0.009$). And the nodal efficiency E_i in FFG.L was significantly positively correlated with H-Y scale ($r = 0.52$, $p = 0.003$).
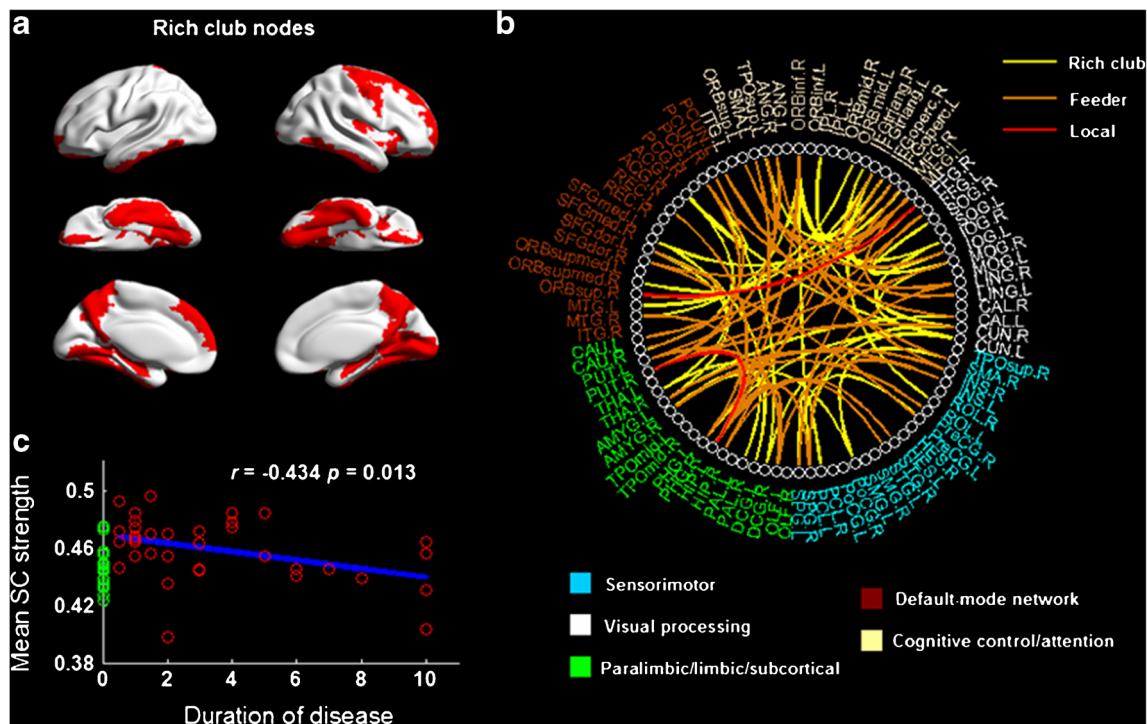

Fig. 2 NBS-derived subnetwork in the PD patients compared to the healthy controls (HC). **a** The identified rich club (hub) regions whose degree $k > 16$ for both PD patients and the controls. **b** Distributions of the rich club, feeder, and local connections within NBS-derived subnetwork. **c** Significant correlation between the structural connectivity (SC) strength of NBS-derived subnetwork and the duration of disease in the PD patients. The symbol ○ in red (green) represents each subject of the PD (HC) group. For illustrative purposes, we also plotted connectivity strength for the controls

Fig. 3 Global parameters of brain structural networks and correlations with clinical variables in PD patients. **a** Bar plot of global parameters. **b** Scatter plot of significant positive correlation between L_p and the duration of disease for the PD patients. **c** Same to (**b**) but for E_{glob}. A significant negative correlation was obtained between E_{glob} and duration of disease. For illustrative purposes, we also plotted global parameters for the controls
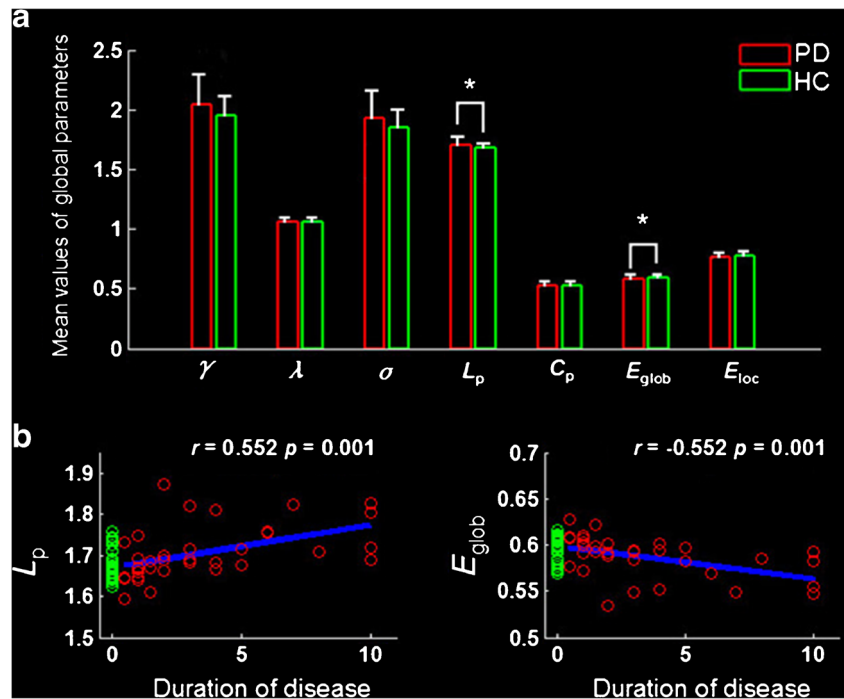
Validation: robustness of our results

In this study, we estimated the robustness of detected changes in both the edge architecture and global properties of PD patients. By taking two other definitions of the edge weights, we reconstructed the brain structural networks and repeated the network analysis. Table S4 and Fig. S1 (supplementary materials) shows the change tends of corresponding global parameters in the PD patients, which is consistent with the main results of this study.

When taking $NOS > 0$ or $NOS \geq 5$ as the thresholds of streamlines counts to define the edge weights, we found that

Table 4 Brain regions showing significantly decreased nodal parameters in the PD patients compared to the healthy controls based on the AAL-90 atlas

Brain regions		p-value		
		Ki	E_i	B_i
Frontal	Precental gyrus (R)	0.045*	0.0004*	0.052
	Olfactory cortex (R)	0.001*	0.0004*	0.019*
	Superior frontal gyrus, medial (L)	0.032*	0.035*	0.119
	Superior frontal gyrus, orbital part (L)	0.497	0.439	0.026*
	Superior frontal gyrus, dorsolateral (R)	0.074	0.562	0.033*
Temporal	Heschl gyrus (L)	0.035*	0.071	0.054
	Fusiform gyrus (L)	0.414	0.350	0.020*
	Fusiform gyrus (R)	0.326	0.303	0.014*
	Middle temporal gyrus (R)	0.035*	0.066	0.017*
	Inferior temporal gyrus (L)	0.055	0.036*	0.139
	Temporal pole: superior temporal gyrus (R)	0.026*	0.042*	0.164
Subcortical	Thalamus (R)	0.065	0.040*	0.295
Occipital	Superior occipital gyrus (L)	0.057	0.027 *	0.149
	Calcarine fissure and surrounding cortex (R)	0.022*	0.004*	0.171
Parietal	Cuneus (R)	0.086	0.030*	0.409
	Paracentral lobule (R)	0.037*	0.138	0.032*

The asterisk (*) indicates significant between-group difference at $p < 0.05$

Abbreviations R (L), right (left) hemisphere; nodal degree (K_i), nodal efficiency (E_i), and nodal betweenness (B_i)

Fig. 4 Scatter plots of significant correlations between nodal parameters and clinical variables in the PD patients. The symbol ○ in red (green) represents each subject of the PD (HC) group. For illustrative purposes, we also plotted the nodal parameters for the controls. Abbreviations: L (R), left (right) hemisphere; H-Y scale, Hoehn and Yahr scale; UPSRS-III, Unified Parkinson Disease Rating Scale-III; MMSE, Mini-Mental State Examination
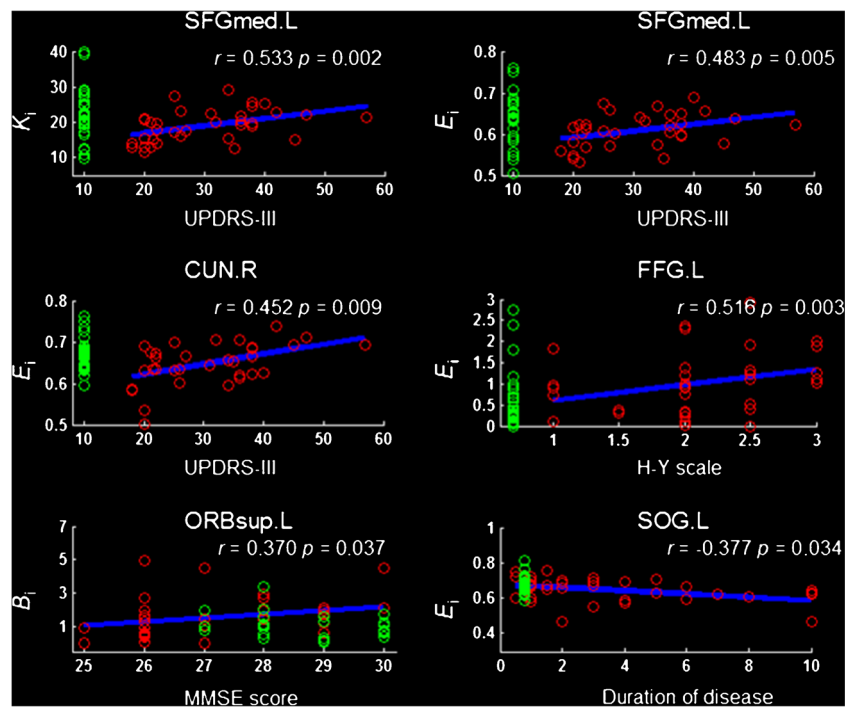
$Feeder^{int}$ and $Local^{int}$ were significantly decreased in PD patients compared to the controls (Supplementary Fig. S2). The same results were obtained when we adopted the other two parcellation schemes, HOA-110 and AAL-1024, to construct brain structural networks. We found the distributions of abnormal structural connectivity of the NBS-derived subnetworks (Supplementary Fig. S3) were similar to those generated from the AAL-90 atlas (see Figs. 1 and 3).

Discussion

In this study, there are three main findings: i) We found that the PD patients showed significant reductions of the integrated feeder connections and the integrated local connections compared to the controls, but no significant between-group difference in the integrated rich club connections. ii) Using the NBS approach, we also detected a significantly decreased subnetwork with 62 nodes and 76 inter-nodal structural connections in the PD patients. iii) For network properties, we found the PD patients had significantly increased shortest path length and decreased global efficiency compared to the controls. And for the changed local properties, there were wide disruptions in the frontal and parietal regions.

Disrupted edge architecture in PD

We detected significantly decreased $Feeder^{int}$ and $Local^{int}$, but not in RC^{int}, in the patients (Fig. 1 and Table 3). This may suggest that the rich club connections, acted as the backbone

of edge architecture, are relatively intact in the PD patients compared to the controls. This result also indicated that non-rich club connections ($Feeder^{int}$ and $Local^{int}$) were prone to be disrupted in the PD patients. This finding of disrupted non-rich club connections was also reported in other brain diseases, such as Huntington's disease and Alzheimer's disease (Daianu et al. 2015; Harrington et al. 2015). Ball et al. (2014) constructed brain structural networks based on diffusion images of PD patients and found significantly decreased short-distance cortico-coritical connections (more specified to the connections among non-hub regions) in premature cohort compared to the term-born cohort. Daianu et al. (2015) analyzed diffusion images in patients with Alzheimer's disease and found that the connections among high-degree regions or hub regions were relatively preserved, while connections among low-degree regions or non-hub regions were significantly disrupted. When selected degree > 16, we identified seventeen rich club regions or hubs, bilateral ORBsup, INS, HIP, LING, FFG, PCUN, PUT, ITG, and right PreCG, for both the PD patients and controls. These results were consistent with several previous fMRI studies (Buckner et al. 2009; Gottlich et al. 2013), which detected prominent hubs in the medical/lateral frontal, lateral parietal, lateral temporal cortex in healthy controls.

In this study, we categorized 90 brain regions (based on the AAL-90 atlas) into sensorimotor, visual processing, attention processing, default mode, and limbic/paralimbic/subcortical (He et al. 2009). However, several fMRI studies (Vincent et al. 2008; Cole et al. 2014) suggested that the frontoparietal network, which was composed by anterior insula, medial

frontal cortex, and lateral frontal and parietal regions, were highly overlapped with attention processing module (Scolari et al. 2015). In this context, we redefined the attention processing module as cognitive control/attention module. First, we detected abnormal structural connections between several striatal regions (i.e., thalamus, putamen and pallidum) and cortical regions (i.e., superior frontal regions and anterior cingulum, Fig. 2 and Table S3) in the PD patients. For the PD patients, dopaminergic and serotonergic dysfunctions (Kim et al. 2002; Dauer and Przedborski 2003) that began from the substantia nigra can impair the physiological microstructures of the basal ganglia and subcortical regions, as well as others overall whole brain. These structural abnormalities of the specific striatal- and cortical-regions are also consistent with previous findings of DTI-related studies in PD patients (Table 5). Previous fMRI/PET studies (Helmich et al. 2010; Jahanshahi et al. 2010) have suggested that the striatal-cortical circuits are closely associated with motor ability in PD patients, typically for the freezing of gait (Shine et al. 2013a, b; Peterson et al. 2014). For example, Shine et al. (2013a) summarized a series of concise findings about the freezing behaviors and proposed a model of basal ganglia impairments for explaining the role of frontostriatal circuit. From the evidence of diffusion images in PD patients, Vercruysse et al. (2015) used a tract-based spatial statistic (TBSS) analysis and found the disrupted striatofrontal tracts through putamen, caudate, and pallidum in PD patients with freezing of gait. Thus, we suggest that the disrupted striatal-cortical structural connections might provide a structural basis for understanding motor deficits in PD patients.

Meanwhile, we also found disrupted connections between limbic/paralimbic regions (especially for the hippocampus, parahippocampus, and amygdala) and other cortical regions (i.e., bilateral insular and left fusiform, Fig. 2b) in PD patients. The hippocampus and parahippocampus are vital regions for working memory ability (Carlesimo et al. 2012) and the amygdala is responsible for emotion processes (Surdhar et al. 2012). Previous structural imaging studies (Nagano-Saito et al. 2005; Melzer et al. 2012) also suggested that the morphology of these brain regions were impaired in PD patients contrasted with healthy individuals. van Mierlo et al. (2015) indicated that decreased gray matter volumes in the right amygdala and bilateral hippocampus were significantly negatively correlated with increased scores on the Beck Depression Inventory in PD patients. As the deficits of emotion and cognitive ability are the core dysfunction of PD patients, therefore, our current findings of structural disconnections between amygdala/hippocampus and other cortical regions in PD patients may provide evidence to illustrate PD disease related to neuropathology changes.

In addition, we detected abnormal structural connections in the frontal cortex based on the NBS approach (Fig. 2b and Table S3). As we know, abnormal frontal-striatal network (Lewis et al. 2003; Owen 2004; Jahanshahi et al. 2010) is primarily related to motor deficits in PD patients, abnormal fronto-parietal network (FPN) (Williams-Gray et al. 2007; Tessitore et al. 2012) is associated with the disabilities of the goal-directed behaviors and executive functions in PD patients, and abnormal salience network (Cools et al. 2010) is connected with the disrupted top-down attention control in PD patients. In addition, several DTI studies in PD patients (see the summary in Table 5) also reported structural alterations in frontal-related regions. For instance, Zheng et al. (2014) conducted correlations analysis between diffusion properties (FA and MD) using region of interest analysis and scores of various cognitive domains (executive function, language, attention, memory, and visuospatial skills) in PD patients. This study showed that executive function in PD patients was significantly positively correlated with FA values and negatively correlated with MD values in frontal WM tracts, while scores on the attention domain was significantly positively correlated with FA values and negatively correlated with MD values cingulum gyrus. Taken together, we infer that the NBS-derived subnetwork may be an effective indicator for depicting the structural basis of motor deficits and cognitive impairments in PD patients.

Abnormal network parameters

We found both the PD patients and the controls exhibited small-worldness (Fig. 3a), indicating their brain structural networks not only had a high local clustering coefficient but also a short path length. However, for global properties (Fig. 3a), PD patients showed significantly decreased global efficiency and increased shortest path length compared to the controls. Global efficiency represents the averaged ability of inter-nodal information transformation over the whole brain. The finding of decreased efficiency may suggest that the inter-nodal organization of the whole brain is unoptimizable in PD patients compared to controls. Notably, a similar result was also reported in previous studies using other imaging modalities (Skidmore et al. 2011; Olde et al. 2014). More detailed, a previous R-fMRI study (Skidmore et al. 2011) constructed brain functional networks, and detected significantly decreased global efficiency in PD patients compared to controls. Olde et al. (2014) performed a longitudinal study on 43 PD patients using the magnetoencephalography (MEG), and detected lower global efficiency in PD patients. The disrupted global properties may reflect the overall information miscommunication in PD patients.

We also observed significantly decreased nodal parameters (nodal strength K_i, nodal efficiency E_i, and nodal betweenness B_i) in 16 brain regions in PD patients compared to controls (Table 4). Four of them, PreCG.R, SFGmed.L, ORBsup.L, and SFGdor.L, are located in the prefrontal cortex involved with attention, executive, and memory abilities in PD patients

Table 5 Overview findings reported in previous DTI studies of patients with Parkinson's disease (PD)

Refs	Subjects and Age	Method	Altered brain regions in PD patients
Shin et al. (2008)	8 HC (51.3 ± 11.1 years) 10 PD (52.3 ± 11.5 years)	VBA	↓ FA: bilateral OFC, PONs, cerebellum, midbrain, parietal, and temporal
Kendi et al. (2008)	13 HC (58.0 ± 7.30 years) 12 PD (62.1 ± 12.7 years)	VBA	↓ FA: bilateral SMA, PreSMA, and ACG
Gattellaro et al. (2009)	10 HC (58.1 ± 8.0 years) 10 PD (63.8 ± 15.7 years)	ROI	↓ FA & ↑ MD: bilateral gCC, and SLF; ↑ MD: bilateral SN, and CG
Zhan et al. (2012)	20 HC (67.2 ± 8.0 years) 12 PD (67.4 ± 8.0 years)	VBA & ROI	↓ FA: PreCG, PUT, SN, SMA, and striatum
Zhang et al. (2011)	25 HC (54.8 ± 9.3 years) 25 PD (54.8 ± 9.8 years)	VBA	↓ FA & ↑ MD: bilateral OFC, OLF, and cerebellum
Kamagata et al. (2012)	20 HC (69.5 ± 6.9 years) 20 PD (69.8 ± 5.9 years) 20 PDD (71.3 ± 5.6 years)	TBSS	↓ FA: PFC WM, and gCC (PDD vs. PD)
Kim et al. (2013)	64 HC (63.0 ± 8.9 years) 64 PD (62.9 ± 9.0 years)	TBSS	↑ MD: CP, CG, CC, CAU, EC, FX, IC, RC, SLF, TR, UF, THA, PUT, PAL, and PCUN
Melzer et al. (2013)	32 HC (70.1 ± 9.0 years) 63 PD (64.0 ± 9.2 years) 18 PDD (73.7 ± 6.5 years) 28 MCI-PD (71.0 ± 7.3 years)	TBSS	↓ FA and ↑ MD: CC (PD vs HC)
Auning et al. (2014)	19 HC (64.6 ± 6.5 years) 18 PD (66.7 ± 5.1 years) 18 MCI-AD (65.6 ± 5.6 years)	VBA & TBSS	↑ RD: bilateral ERC WM, LING, and PCUN (PD vs HC)
Agosta et al. (2014)	33 HC (64.0 ± 7.3 years) 43 PD (65.8 ± 7.9 years) 13 PD-Cu (63.9 ± 7.1 years) 30 MCI-PD (66.6 ± 8.2 years)	TBSS	↓ FA: CR, CC, and SLF (MCI-PD vs HC) ↓ FA: CR, gCC, bCC, UF, and SLF (MCI-PD vs PD-Cu)
Zheng et al. (2014)	16 PD (62.2 ± 9.6 years)	VBA & ROIs	↓ FA & ↑ MD: FA and MD of IC, gCC correlated with the executive function; FA and MD of frontal WM, CG corrected with the language and attentional performance ↑ MD: MD of FX correlated with the memory impairment

Abbreviations ↑ PD > HC, ↓ PD < HC, *MCI* mild cognitive impairment, *PD-Cu* PD patients with unimpaired cognition, *PDD* PD patients with dementia, *ROI* region of interest, *TBSS* tract-based spatial statistics, *VBA* voxel-based analysis, *WM* white matter, *CG* cingulate gyrus, *ACG* anterior cingulate gyrus, *CC* corpus callosum, *bCC* body of corpus callosum, *gCC* genu of corpus callosum, *CAU* caudate, *CP* cerebral peduncle, *CR* corona radiata, *EC* external capsule, *ERC* entorhinal cortex, *FX* fornix, *IC* internal capsule, *LING* lingual gyrus, *OFC* orbitofrontal cortex, *OLF* olfactory, *PCUN* precuneus, *PFC* prefrontal cortex, *PUT* putamen, *PreSMA* pre-supplementary motor area, *PreCG* precentral gyrus, *SLF* superior longitudinal fasciculus, *SMA* supplementary motor area, *SN* substantia nigra, *THA* thalamus, *TR* thalamic radiations, *UF* uncinate fasciculus, *FA* fractional anisotropy, *MD* mean diffusivity, *RD* radial diffusivity

(Karagulle et al. 2008; Kamagata et al. 2012). Decreased nodal parameters (K_i, E_i, or B_i) in another four brain regions, including bilateral FFG, right CAL, and left SOG may reflect abnormalities of visual processing in PD patients (Meppelink et al. 2009; Tinaz et al. 2011). Noticeably, all of these three nodal parameters (K_i, E_i, and B_i) in PD patients showed significant decreases in the right olfactory cortex, which is considered as a potential biomarker of early-stage PD by several R-fMRI studies (Rolheiser et al. 2011; Zhang et al. 2011). Thus, our findings of abnormal nodal parameters in patients might provide the locally pathological impairments in Parkinson's disease.

Correlations between network parameters and clinical variables

Correlation analysis showed the connectivity strength of NBS-derived subnetwork was significantly negatively correlated with the duration of disease in patients (Fig. 2c). This indicated that the longer the patients suffered from PD disease, the weaker the inter-nodal WM connectivity. For global properties, we found the increased shortest path length L_p was significantly positively and the decreased global efficiency E_{glob} was significantly negatively correlated with disease duration in PD patients (Fig. 3b). This means that the duration of disease affects

the network connectivity of PD patients. These results are consistent with previous studies (Huang et al. 2007; Olde et al. 2014) the duration of illness could worsen brain microstructures of patients with Parkinson's disease, especially for the midbrain and striatal regions. More detailed, Huang et al. (2007) performed a longitudinal PET study for early stage PD patients at baseline, 24 and 48 moths to compared changed network metabolisms that were associated with motor and cognitive abilities. With increasing duration of disease, they found increasing metabolisms in subthalamic nucles, internal globus pallius, dorsal pons, and primary motor cortex, while decreasing metabolisms in prefrontal and inferior parietal regions. Olde et al. (2014) acquired the magnetoencephalography (MEG) data of 70 PD patients for 4 years and detected differences of network topology using graph theory. Their findings suggested that disrupted local efficient and network decentralization are early characteristics of Parkinson's disease that continue to progress over time, together with decreased global efficiency.

Limitations

Our study has several limiting factors. First, the selection of brain parcellation schemes for constructing brain networks may bias the results of network analysis. Several previous studies (Wang et al. 2009; Zalesky et al. 2010b) have suggested that it is quite controversial to select which brain parcellation schemes to construct whole-brain networks. And various brain parcellation schemes, including the Harvard–Oxford Atlas (HOA-110) and LPBA40-atlas (LONI Probabilistic Brain Atlas), have been adopted in constructing brain structural networks (Cao et al. 2013). In the current study, we selected three brain schemes, AAL-90, HOA-110, and AAL-1,024, to test the robustness of our results (Supplement Table S4). Second, we collected the DTI data using an 8-channel rather than 32-channel coil as we were limited to realistic situations. Several previous studies (Parikh et al. 2011; Salomon et al. 2014) suggested that using a multi-channel phased-array head coil with a parallel imaging technique can accelerate acquisition and reduce susceptibility artifacts, especially in the frontal cortex. In the future, we need adopt advanced DTI techniques to reduce susceptibility artifacts and to reduce the scanning time. Third, the estimation of inter-regional structural connectivity may be affected by our choice of fiber tracking algorithm. In this study, we took the (FACT) algorithm (Mori and van Zijl 2002), a single-tensor deterministic fiber tracking approach to draw fiber streamlines. Previous studies (Alexander et al. 2001; Behrens et al. 2003) have suggested that the single-tenor model is incapable of resolving complex fiber configurations, such as crossing, kissing, or merged fiber bundles. Therefore, some advanced algorithms or imaging sequences, including a probabilistic tractography algorithm (Behrens et al. 2007) and diffusion

spectrum imaging (DSI) technique (Wedeen et al. 2012), were introduced to resolve the question of complex fiber configurations for accurately measuring the fiber tracking. In the end, we did not use any multiple comparisons correction in analyzing the changes of global or nodal parameters. To remedy this issue, we adopted a two-sample t-test with a nonparametric permutation test (1,000 repetitions) to assess the statistical significances in our study (Nichols and Holmes 2002). Our results, to some extent, are more tended to an exploratory study.

In this study, we used diffusion tensor imaging and graph theoretical approach to detect the abnormalities of brain structural networks in PD patients. The structural disconnections of edge architecture in the PD patients were more concentrated among non-hub regions involving the limbic/paralimbic/subcortical and cognitive control/attention modules. For network properties, PD patients showed reduced global efficiency and increased short path length, as well as decreased local properties mainly in the frontal and parietal regions. Thus, our main findings suggest that the backbone of brain networks in PD patients was still intact, but the others were impaired companied with disrupted network properties. Our study also suggests that the edge architecture and topological properties would be an effective way to depict PD-related cognitive and motor dysfunction alterations.

References

Agosta, F., Canu, E., Stefanova, E., Sarro, L., Tomic, A., Spica, V., Comi, G., Kostic, V. S., & Filippi, M. (2014). Mild cognitive impairment in Parkinson's disease is associated with a distributed pattern of brain white matter damage. *Human Brain Mapping, 35*(5), 1921–1929.

Alexander, A. L., Hasan, K. M., Lazar, M., Tsuruda, J. S., & Parker, D. L. (2001). Analysis of partial volume effects in diffusion-tensor MRI. *Magnetic Resonance Imaging, 45*(5), 770–780.

Auning, E., Kjærvik, V. K., Selnes, P., Aarsland, D., Haram, A., Bjørnerud, A., Hessen, E., Esnaashari, A., & Fladby, T. (2014). White matter integrity and cognition in Parkinson's disease: a cross-sectional study. *BMJ open, 4*(1), e003976.

Ball, G., Aljabar, P., Zebari, S., Tusor, N., Arichi, T., Merchant, N., Robinson, E. C., Ogundipe, E., Rueckert, D., Edwards, A. D., & Counsell, S. J. (2014). Rich-club organization of the newborn human brain. *PNAS, 111*(20), 7456–7461.

Behrens, T., Woolrich, M., Jenkinson, M., Johansen-Berg, H., Nunes, R., Clare, S., Matthews, P., Brady, J., & Smith, S. (2003). Characterization and propagation of uncertainty in diffusion-weighted MR imaging. *Magnetic Resonance in Medicine, 50*(5), 1077–1088.

Behrens, T., Berg, H. J., Jbabdi, S., Rushworth, M., & Woolrich, M. (2007). Probabilistic diffusion tractography with multiple fibre orientations: what can we gain? *NeuroImage, 34*(1), 144–155.

Buckner, R. L., Sepulcre, J., Talukdar, T., Krienen, F. M., Liu, H., Hedden, T., Andrews-Hanna, J. R., Sperling, R. A., & Johnson, K. A. (2009). Cortical hubs revealed by intrinsic functional connectivity: mapping, assessment of stability, and relation to Alzheimer's disease. *Journal of Neuroscience, 29*(6), 1860–1873.

Cao, Q., Shu, N., An, L., Wang, P., Sun, L., Xia, M. R., Wang, J. H., Gong, G. L., Zang, Y. F., Wang, Y. F., & He, Y. (2013). Probabilistic diffusion tractography and graph theory analysis reveal abnormal white matter structural connectivity networks in drug-naive boys with attention deficit/hyperactivity disorder. *Journal of Neuroscience, 33*(26), 10676–10687.

Carlesimo, G. A., Piras, F., Assogna, F., Pontieri, F. E., Caltagirone, C., & Spalletta, G. (2012). Hippocampal abnormalities and memory deficits in Parkinson disease: a multimodal imaging study. *Neurology, 78*(24), 1939–1945.

Chaudhuri, K., Healy, D. G., & Schapira, A. H. (2006). Non-motor symptoms of Parkinson's disease: diagnosis and management. *Lancet Neurology, 5*(3), 235–245.

Cheng, H., Wang, Y., Sheng, J., Kronenberger, W. G., Mathews, V. P., Hummer, T. A., & Saykin, A. J. (2012). Characteristics and variability of structural networks derived from diffusion tensor imaging. *NeuroImage, 61*(4), 1153–1164.

Cole, M. W., Repovs, G., & Anticevic, A. (2014). The frontoparietal control system: a central role in mental health. *The Neuroscientist, 20*(6), 652–664.

Collin, G., Kahn, R. S., de Reus, M. A., Cahn, W., & van den Heuvel, M. P. (2014a). Impaired rich club connectivity in unaffected siblings of schizophrenia patients. *Schizophrenia Bulletin, 40*(2), 438–448.

Collin, G., Sporns, O., Mandl, R. C., & van den Heuvel, M. P. (2014b). Structural and functional aspects relating to cost and benefit of rich club organization in the human cerebral cortex. *Cerebral Cortex, 24*(9), 2258–2267.

Cools, R., Rogers, R., Barker, R. A., & Robbins, T. W. (2010). Top-down attentional control in Parkinson's disease: salient considerations. *Journal Cognitive Neuroscience, 22*(5), 848–859.

Crossley, N. A., Mechelli, A., Scott, J., Carletti, F., Fox, P. T., McGuire, P., & Bullmore, E. T. (2014). The hubs of the human connectome are generally implicated in the anatomy of brain disorders. *Brain, 137*(Pt 8), 2382–2395.

Daianu, M., Jahanshad, N., Nir, T. M., Jack, C. R., Jr., Weiner, M. W., Bernstein, M. A., Thompson, P. M., & I Alzheimer's Disease Neuroimaging. (2015). Rich club analysis in the Alzheimer's disease connectome reveals a relatively undisturbed structural core network. *Human Brain Mapping, 36*(8), 3087–3103.

Daniel, S. E., & Lees, A. J. (1993). Parkinson's disease society brain bank, London: overview and research. *Journal of Neural Transmission Supplementum, 39*, 165–172.

Dauer, W., & Przedborski, S. (2003). Parkinson's disease: mechanisms and models. *Neuron, 39*(6), 889–909.

Diederich, N. J., Fenelon, G., Stebbins, G., & Goetz, C. G. (2009). Hallucinations in Parkinson disease. *Nature Reviews Neurology, 5*(6), 331–342.

Drui, G., Carnicella, S., Carcenac, C., Favier, M., Bertrand, A., Boulet, S., & Savasta, M. (2014). Loss of dopaminergic nigrostriatal neurons accounts for the motivational and affective deficits in Parkinson's disease. *Molecular Psychiatry, 19*(3), 358–367.

Gattellaro, G., Minati, L., Grisoli, M., Mariani, C., Carella, F., Osio, M., Ciceri, E., Albanese, A., & Bruzzone, M. G. (2009). White matter involvement in idiopathic Parkinson disease: a diffusion tensor imaging study. *American Journal of Neuroradiology, 30*(6), 1222–1226.

Gong, G., He, Y., Concha, L., Lebel, C., Gross, D. W., Evans, A. C., & Beaulieu, C. (2009). Mapping anatomical connectivity patterns of human cerebral cortex using in vivo diffusion tensor imaging tractography. *Cerebral Cortex, 19*, 524–536.

Gottlich, M., Munte, T. F., Heldmann, M., Kasten, M., Hagenah, J., & Kramer, U. M. (2013). Altered resting state brain networks in Parkinson's disease. *PloS One, 8*(10), e77336.

Hagmann, P., Kurant, M., Gigandet, X., Thiran, P., Wedeen, V. J., Meuli, R., & Thiran, J. P. (2007). Mapping human whole-brain structural networks with diffusion MRI. *PloS One, 2*(7), e597.

Harrington, D. L., Rubinov, M., Durgerian, S., Mourany, L., Reece, C., Koenig, K., Bullmore, E., Long, J. D., Paulsen, J. S., P-HiotHS Group, & Rao, S. M. (2015). Network topology and functional connectivity disturbances precede the onset of Huntington's disease. *Brain, 138*(Pt 8), 2332–2346.

He, Y., Wang, J. H., Wang, L., Chen, Z. J., Yan, C., Yang, H., Tang, H., Zhu, C., Gong, Q., Zang, Y., & Evans, A. C. (2009). Uncovering intrinsic modular organization of spontaneous brain activity in humans. *PloS One, 4*(4), e5226.

Helmich, R. C., Derikx, L. C., Bakker, M., Scheeringa, R., Bloem, B. R., & Toni, I. (2010). Spatial remapping of cortico-striatal connectivity in Parkinson's disease. *Cerebral Cortex, 20*(5), 1175–1186.

Huang, C., Tang, C., Feigin, A., Lesser, M., Ma, Y., Pourfar, M., Dhawan, V., & Eidelberg, D. (2007). Changes in network activity with the progression of Parkinson's disease. *Brain, 130*(Pt 7), 1834–1846.

Jahanshahi, M., Jones, C. R., Zijlmans, J., Katzenschlager, R., Lee, L., Quinn, N., Frith, C. D., & Lees, A. J. (2010). Dopaminergic modulation of striato-frontal connectivity during motor timing in Parkinson's disease. *Brain, 133*(Pt 3), 727–745.

Jankovic, J. (2008). Parkinson's disease: clinical features and diagnosis. *Journal of Neurology, Neurosurgery, and Psychiatry, 79*(4), 368–376.

Kamagata, K., Motoi, Y., Abe, O., Shimoji, K., Hori, M., Nakanishi, A., Sano, T., Kuwatsuru, R., Aoki, S., & Hattori, N. (2012). White matter alteration of the cingulum in Parkinson disease with and without dementia: evaluation by diffusion tensor tract–specific analysis. *American Journal of Neuroradiology, 33*(5), 890–895.

Karagulle, K. A. T., Lehericy, S., Luciana, M., Ugurbil, K., & Tuite, P. (2008). Altered diffusion in the frontal lobe in Parkinson disease. *American Journal of Neuroradiology, 29*(3), 501–505.

Kendi, A. K., Lehericy, S., Luciana, M., Ugurbil, K., & Tuite, P. (2008). Altered diffusion in the frontal lobe in Parkinson disease. *American Journal of Neuroradiology, 29*(3), 501–505.

Kim, J. H., Auerbach, J. M., Rodriguez-Gomez, J. A., Velasco, I., Gavin, D., Lumelsky, N., Lee, S. H., Nguyen, J., Sanchez-Pernaute, R., Bankiewicz, K., & McKay, R. (2002). Dopamine neurons derived from embryonic stem cells function in an animal model of Parkinson's disease. *Nature, 418*(6893), 50–56.

Kim, H. J., Kim, S. J., Kim, H. S., Choi, C. G., Kim, N., Han, S., Jang, E. H., Chung, S. J., & Lee, C. S. (2013). Alterations of mean diffusivity in brain white matter and deep gray matter in Parkinson's disease. *Neuroscience letters, 550*, 64–68.

Kocher, M., Gleichgerrcht, E., Nesland, T., Rorden, E., Fridriksson, J., Spampinato, M. V. & Bonilha, L. (2015). Individual variability in the anatomical distribution of nodes participating in rich club structural networks. *Frontiers in Neural Circuits*, 916.

Latora, V., & Marchiori, M. (2001). Efficient behavior of small-world networks. *Physical review letters, 87*(19), 198701.

Le Bihan, D., & Johansen-Berg, H. (2012). Diffusion MRI at 25: exploring brain tissue structure and function. *NeuroImage, 61*(2), 324–341.

Lees, A. J., Hardy, J., & Revesz, T. (2009). Parkinson's disease. *Lancet, 373*(9680), 2055–2066.

Lewis, S. J., Dove, A., Robbins, T. W., Barker, R. A., & Owen, A. M. (2003). Cognitive impairments in early Parkinson's disease are accompanied by reductions in activity in frontostriatal neural circuitry. *Journal of Neuroscience, 23*(15), 6351–6356.

Lo, C. Y., Wang, P. N., Chou, K. H., Wang, J., He, Y., & Lin, C. P. (2010). Diffusion tensor tractography reveals abnormal topological organization in structural cortical networks in Alzheimer's disease. *Journal of Neuroscience, 30*(50), 16876–16885.

Melzer, T. R., Watts, R., MacAskill, M. R., Pitcher, T. L., Livingston, L., Keenan, R. J., Dalrymple-Alford, J. C., & Anderson, T. J. (2012). Grey matter atrophy in cognitively impaired Parkinson's disease. *Journal of Neurology, Neurosurgery, and Psychiatry, 83*(2), 188–194.

Melzer, T. R., Watts, R., MacAskill, M. R., Pitcher, T. L., Livingston, L., Keenan, R. J., Dalrymple-Alford, J. C., & Anderson, T. J. (2013). White matter microstructure deteriorates across cognitive stages in Parkinson disease. *Neurology, 80*(20), 1841–1849.

Meppelink, A. M., de Jong, B. M., Renken, R., Leenders, K. L., Cornelissen, F. W., & van Laar, T. (2009). Impaired visual processing preceding image recognition in Parkinson's disease patients with visual hallucinations. *Brain, 132*(11), 2980–2993.

Mori, S., & van Zijl, P. C. (2002). Fiber tracking: principles and strategies - a technical review. *NMR in Biomedicine, 15*(7–8), 468–480.

Nagano-Saito, A., Washimi, Y., Arahata, Y., Kachi, T., Lerch, J. P., Evans, A. C., Dagher, A., & Ito, K. (2005). Cerebral atrophy and its relation to cognitive impairment in Parkinson disease. *Neurology, 64*(2), 224–229.

Nichols, T. E., & Holmes, A. P. (2002). Nonparametric permutation tests for functional neuroimaging: a primer with examples. *Human Brain Mapping, 15*(1), 1–25.

Olde, D. K. T., Hillebrand, A., Stoffers, D., Deijen, J. B., Twisk, J. W., Stam, C. J., & Berendse, H. W. (2014). Disrupted brain network topology in Parkinson's disease: a longitudinal magnetoencephalography study. *Brain, 137*(Pt 1), 197–207.

Onnela, J. P., Saramäki, J., Kertész, J., & Kaski, K. (2005). Intensity and coherence of motifs in weighted complex networks. *Physical Review E, 71*(6), 065103.

Owen, A. M. (2004). Cognitive dysfunction in Parkinson's disease: the role of frontostriatal circuitry. *The Neuroscientist, 10*(6), 525–537.

Parikh, P. T., Sandhu, G. S., Blackham, K. A., Coffey, M. D., Hsu, D., Liu, K., Jesberger, J., Griswold, M., & Sunshine, J. L. (2011). Evaluation of image quality of a 32-channel versus a 12-channel head coil at 1.5 T for MR imaging of the brain. *American Journal of Neuroradiology, 32*(2), 365–373.

Peterson, D. S., Pickett, K. A., Duncan, R., Perlmutter, J., & Earhart, G. M. (2014). Gait-related brain activity in people with Parkinson disease with freezing of gait. *PloS One, 9*(3), e90634.

Rolheiser, T. M., Fulton, H. G., Good, K. P., Fisk, J. D., McKelvey, J. R., Scherfler, C., Khan, N. M., Leslie, R. A., & Robertson, H. A. (2011). Diffusion tensor imaging and olfactory identification testing in early-stage Parkinson's disease. *Journal of Neurology, 258*(7), 1254–1260.

Rubinov, M., & Sporns, O. (2010). Complex network measures of brain connectivity: uses and interpretations. *NeuroImage, 52*(3), 1059–1069.

Salomon, R., Darulova, J., Narsude, M., & van der Zwaag, W. (2014). Comparison of an 8-channel and a 32-channel coil for high-resolution fMRI at 7 T. *Brain Topography, 27*(2), 209–212.

Scolari, M., Seidl-Rathkopf, K. N, & Kastner, S. (2015). Functions of the human frontoparietal attention network: evidence from neuroimaging. *Current Opinion in Behavioral Sciences*, 132–39.

Shin, D. H., Han, B. S., Kim, H. S., & Lee, P. H. (2008). Diffusion tensor imaging in patients with essential tremor. *American Journal of Neuroradiology, 29*(1), 151–153.

Shine, J. M., Matar, E., Ward, P. B., Frank, M. J., Moustafa, A. A., Pearson, M., Naismith, S. L., & Lewis, S. J. (2013a). Freezing of gait in Parkinson's disease is associated with functional decoupling between the cognitive control network and the basal ganglia. *Brain, 136*(Pt 12), 3671–3681.

Shine, J. M., Moustafa, A. A., Matar, E., Frank, M. J., & Lewis, S. J. (2013). The role of frontostriatal impairment in freezing of gait in Parkinson's disease. *Frontiers in Systems Neuroscience*, 761.

Shu, N., Liu, Y., Li, K., Duan, Y., Wang, J., Yu, C., Dong, H., Ye, J., & He, Y. (2011). Diffusion tensor tractography reveals disrupted topological efficiency in white matter structural networks in multiple sclerosis. *Cerebral Cortex, 21*(11), 2565–2577.

Skidmore, F., Korenkevych, D., Liu, Y., He, G., Bullmore, E., & Pardalos, P. M. (2011). Connectivity brain networks based on wavelet correlation analysis in Parkinson fMRI data. *Neuroscience Letters, 499*(1), 47–51.

Surdhar, I., Gee, M., Bouchard, T., Coupland, N., Malykhin, N., & Camicioli, R. (2012). Intact limbic-prefrontal connections and reduced amygdala volumes in Parkinson's disease with mild depressive symptoms. *Parkinsonism & Related Disorders, 18*(7), 809–813.

Tessitore, A., Amboni, M., Esposito, F., Russo, A., Picillo, M., Marcuccio, L., Pellecchia, M. T., Vitale, C., Cirillo, M., Tedeschi, G., & Barone, P. (2012). Resting-state brain connectivity in patients with Parkinson's disease and freezing of gait. *Parkinsonism & Related Disorders, 18*(6), 781–787.

Tewarie, P., Steenwijk, M. D., Tijms, B. M., Daams, M., Balk, L. J., Stam, C. J., Uitdehaag, B. M., Polman, C. H., Geurts, J. J., Barkhof, F., Pouwels, P. J., Vrenken, H., & Hillebrand, A. (2014). Disruption of structural and functional networks in long-standing multiple sclerosis. *Human Brain Mapping, 35*(12), 5946–5961.

Tian, L., Wang, J., Yan, C., & He, Y. (2011). Hemisphere- and gender-related differences in small-world brain networks: a resting-state functional MRI study. *NeuroImage, 54*(1), 191–202.

Tinaz, S., Courtney, M. G., & Stern, C. E. (2011). Focal cortical and subcortical atrophy in early Parkinson's disease. *Movement Disorders, 26*(3), 436–441.

Tzourio-Mazoyer, N., Landeau, B., Papathanassiou, D., Crivello, F., Etard, O., Delcroix, N., Mazoyer, B., & Joliot, M. (2002). Automated anatomical labeling of activations in SPM using a macroscopic anatomical parcellation of the MNI MRI single-subject brain. *NeuroImage, 15*(1), 273–289.

van den Heuvel, M. P., & Sporns, O. (2011). Rich-club organization of the human connectome. *Journal of Neuroscience, 31*(44), 15775–15786.

van den Heuvel, M. P., Kahn, R. S., Goni, J., & Sporns, O. (2012). High-cost, high-capacity backbone for global brain communication. *PNAS, 109*(28), 11372–11377.

van den Heuvel, M. P., Sporns, O., Collin, G., Scheewe, T., Mandl, R. C., Cahn, W., Goni, J., Hulshoff Pol, H. E., & Kahn, R. S. (2013). Abnormal rich club organization and functional brain dynamics in schizophrenia. *JAMA Psychiatry, 70*(8), 783–792.

van Mierlo, T. J., Chung, C., Foncke, E. M., Berendse, H. W., & van den Heuvel, O. A. (2015). Depressive symptoms in Parkinson's disease are related to decreased hippocampus and amygdala volume. *Movement Disorders, 30*(2), 245–252.

Vercruysse, S., Leunissen, I., Vervoort, G., Vandenberghe, W., Swinnen, S., & Nieuwboer, A. (2015). Microstructural changes in white matter associated with freezing of gait in Parkinson's disease. *Movement Disorders, 30*(4), 567–576.

Vincent, J. L., Kahn, I., Snyder, A. Z., Raichle, M. E., & Buckner, R. L. (2008). Evidence for a frontoparietal control system revealed by intrinsic functional connectivity. *Journal of Neurophysiology, 100*(6), 3328–3342.

Wang, J., Wang, L., Zang, Y., Yang, H., Tang, H., Gong, Q., Chen, Z., Zhu, C., & He, Y. (2009). Parcellation-dependent small-world brain functional networks: a resting-state fMRI study. *Human Brain Mapping, 30*(5), 1511–1523.

Wang, J., Zuo, X., Dai, Z., Xia, M., Zhao, Z., Zhao, X., Jia, J., Han, Y., & He, Y. (2013). Disrupted functional brain connectome in individuals at risk for Alzheimer's disease. *Biological Psychiatry, 73*(5), 472–481.

Wang, J., Wang, X., Xia, M., Liao, X., Evans, A., & He, Y. (2015). GRETNA: a graph theoretical network analysis toolbox for imaging connectomics. *Frontiers in Human Neuroscience*, 9386.

Watts, D. J., & Strogatz, S. H. (1998). Collective dynamics of 'small-world' networks. *Nature, 393*(6684), 440–442.

Wedeen, V. J., Rosene, D. L., Wang, R., Dai, G., Mortazavi, F., Hagmann, P., Kaas, J. H., & Tseng, W.-Y. I. (2012). The geometric structure of the brain fiber pathways. *Science, 335*(6076), 1628–1634.

Williams-Gray, C. H., Hampshire, A., Robbins, T. W., Owen, A. M., & Barker, R. A. (2007). Catechol O-methyltransferase Val158Met genotype influences frontoparietal activity during planning in patients with Parkinson's disease. *Journal of Neuroscience, 27*(18), 4832–4838.

Zalesky, A., Fornito, A., & Bullmore, E. T. (2010a). Network-based statistic: identifying differences in brain networks. *NeuroImage, 53*(4), 1197–1207.

Zalesky, A., Fornito, A., Harding, I. H., Cocchi, L., Yücel, M., Pantelis, C., & Bullmore, E. T. (2010b). Whole-brain anatomical networks: does the choice of nodes matter? *NeuroImage, 50*(3), 970–983.

Zalesky, A., Fornito, A., Seal, M. L., Cocchi, L., Westin, C. F., Bullmore, E. T., Egan, G. F., & Pantelis, C. (2011). Disrupted axonal fiber connectivity in schizophrenia. *Biological Psychiatry, 69*(1), 80–89.

Zhan, W., Kang, G. A., Glass, G. A., Zhang, Y., Shirley, C., Millin, R., Possin, K. L., Nezamzadeh, M., Weiner, M. W., Marks Jr, W. J., & Schuff, N. (2012). Regional alterations of brain microstructure in Parkinson's disease using diffusion tensor imaging. *Movement disorders, 27*(1), 90–97.

Zhang, K., Yu, C., Zhang, Y., Wu, X., Zhu, C., Chan, P., & Li, K. (2011). Voxel-based analysis of diffusion tensor indices in the brain in patients with Parkinson's disease. *European Journal of Radiology, 77*(2), 269–273.

Zhang, R., Wei, Q., Kang, Z., Zalesky, A., Li, M., Xu, Y., Li, L., Wang, J., Zheng, L., Wang, B., Zhao, J., Zhang, J., & Huang, R. (2015). Disrupted brain anatomical connectivity in medication-naive patients with first-episode schizophrenia. *Brain Structure and Function, 220*(2), 1145–1159.

Zheng, Z., Shemmassian, S., Wijekoon, C., Kim, W., Bookheimer, S. Y., & Pouratian, N. (2014). DTI correlates of distinct cognitive impairments in Parkinson's disease. *Human Brain Mapping, 35*(4), 1325–1333.

Zhong, S., He, Y., & Gong, G. (2015). Convergence and divergence across construction methods for human brain white matter networks: an assessment based on individual differences. *Human Brain Mapping, 36*(5), 1995–2013.